Preprint of

Application of Optimal Control Theory to the Design of Broadband Excitation Pulses for High Resolution NMR

T. E. Skinner, T. O. Reiss, B. Luy, N. Khaneja, S. J. Glaser

J. Magn. Reson. 163, 8-15 (2003).

Application of Optimal Control Theory to the Design of Broadband Excitation Pulses for High Resolution NMR

Thomas E. Skinner[1], Timo O. Reiss[2], Burkhard Luy[2], Navin Khaneja[3], Steffen J. Glaser[2]

[1] *Physics Department, Wright State University, Dayton, OH 45435;* [2] *Institut für Organische Chemie und Biochemie II, Technische Universität München, Lichtenbergstr. 4, 85747 Garching, Germany; and* [3] *Division of Engineering and Applied Sciences, Harvard University, 29 Oxford Street, Cambridge, MA 02138*

E-mail: thomas.skinner@wright.edu, glaser@ch.tum.de

Received ; revised ; accepted .

Optimal control theory is considered as a methodology for pulse sequence design in NMR. It provides the flexibility for systematically imposing desirable constraints on spin system evolution and therefore has a wealth of applications. We have chosen an elementary example to illustrate the capabilities of the optimal control formalism: broadband, constant phase excitation which tolerates miscalibration of RF power and variations in RF homogeneity relevant for standard high-resolution probes. The chosen design criteria were transformation of $I_z \rightarrow I_x$ over resonance offsets of ± 20 kHz and RF variability of $\pm 5\%$, with a pulse length of 2 ms. Simulations of the resulting pulse transform $I_z \rightarrow 0.995 I_x$ over the target ranges in resonance offset and RF variability. Acceptably uniform excitation is obtained over a much larger range of RF variability ($\sim 45\%$) than the strict design limits. The pulse performs well in simulations that include homonuclear and heteronuclear J-couplings. Experimental spectra obtained from 100% ^{13}C-labeled lysine show only minimal coupling effects, in excellent agreement with the simulations. By increasing pulse power and reducing pulse length, we demonstrate experimental excitation of ^{1}H over ± 32 kHz, with phase variations in the spectra $< 8^\circ$ and peak amplitudes $> 93\%$ of maximum. Further improvements in *B*roadband *E*xcitation *B*y *O*ptimized *P*ulses (BEBOP) may be possible by applying more sophisticated implementations of the optimal control formalism.

Key Words: broadband excitation, BEBOP.

INTRODUCTION

The excitation pulse is indispensible in FT-NMR. There is no signal without first transforming some of the initial sample polarization to the transverse plane. Although the high fields employed in modern spectrometers increase sensitivity and spectral resolution, they also require a concomitant increase in excitation bandwidth. The workhorse of NMR pulses is probably the simple hard pulse, which excites transverse magnetization $I_z \rightarrow 0.95 I_{xy}$ over a bandwidth which is roughly a factor of 2.5 times the applied RF amplitude. The phase of the final magnetization is approximately linear as a function of resonance offset and can be easily corrected in 1D spectra. The phase-correction procedure for multi-dimensional spectroscopy is less simple and becomes more problematic for applications involving long pulse trains and multiple coherence pathways. Moreover, the bandwidth of the pulse is considerably reduced in the presence of RF inhomogeneity or miscalibration. Of additional relevance is the approach of 1 GHz spectroscopy, which sets a target bandwidth of ~ 50 kHz for excitation of the entire 200 ppm ^{13}C chemical shift range. The requisite 20–25 kHz (12.5–10 μs) hard pulse exceeds the capabilities of most ^{13}C probes. Broadband excitation pulses which incorporate the added convenience of constant-phase transverse magnetization are therefore of more than passing interest. Robust pulses which tolerate RF inhomogeneity or miscalibration are also desirable.

Many methods exist for reducing the phase variation of the excited magnetization as a function of resonance offset [1, 2, 3, 4, 5, 6, 7, 8, 9, 10, 11, 12, 13]. As a benchmark for comparing pulse performance to the standard hard pulse, consider a transverse magnetization equal to at least 95% of the initial equilibrium value with a phase roll of up to 4° over the offset range. Typically, composite pulses satisfying this standard achieve excitation bandwidths that are less than $\pm 50\%$ of the applied RF field. Slightly better performance is obtained for excitation pulses derived using the Floquet formalism [9]. A commonly used figure-of-merit (FOM), defined as the total excitation bandwidth satisfy-

ing the benchmark divided by the peak RF amplitude, is less than 1.5 for this group of pulses. The FOM decreases significantly if the standard includes dual compensation for the effects of resonance offset and RF inhomogeneity.

More efficient excitation is obtainable using phase-alternated composite pulses [6] (FOM = 2.5). Polychromatic pulses [10] have a low FOM = 0.8 according to strict adherence to the benchmark, but this improves dramatically to FOM = 2.2 if a phase roll of up to 6° is allowed. Although RF compensation was not part of the design criteria, both pulses have some serendipitous tolerance to RF inhomogeneity. However, no procedure was provided for incorporating tolerance to RF inhomogeneity directly in these pulses, and the FOM also decreases if the RF is miscalibrated.

The broadband capabilities of adiabatic pulses have been applied to develop methods for refocusing the phase of the excited transverse magnetization [7, 8, 11, 12]. However, these techniques work well only for ideal RF values, which, again, highlights the difficulty of achieving tolerance to variations in RF and resonance offset simultaneously. A clever solution to this problem, with modest tolerance to RF inhomogeneity, has been proposed [13] using hyperbolic secant pulses [14, 15, 16] for excitation and refocusing (FOM = $\sim$ 4.5). However, this pulse shape characteristically operates at very low RF values for a significant fraction of the pulse. The resulting ABSTRUSE sequence is 12 ms long, and even a pulse half this length may be subject to the effects of J-modulation during the pulse. Relaxation is also an important issue during application of long pulses.

Dual compensation for RF and chemical shift variation, with minimal J-modulation and relaxation during the pulse, is thus a difficult design problem. A systematic procedure for achieving all these goals simultaneously is the topic of this paper. It provides the possibility for significant improvements in pulse performance. We present results of our initial attempts using optimal control theory [17, 18, 19, 20] to design, for use in high-resolution NMR, broadband 90° pulses which excite transverse magnetization of nearly constant phase with tolerance to RF miscalibration and inhomogeneity. We first provide an overview of the method, sufficient to give insight into the optimization procedure. Details of the basic theory relevant for NMR of simple spin systems (ignoring coupling effects) can be found in Refs. [21, 22], applied to narrowband selective excitation for imaging applications. An alternative to optimal control for simple spin systems can be found in [23]. However, this method is not easily extended to more general systems involving coupled spins, and our long-term goals encompass a variety of more general applications which require the flexibility and extensibility found in optimal control theory. The overview material is followed by discussion of a 2 ms pulse obtained using the procedure, where we demonstrate its successful performance over a bandwidth of 40 kHz. The pulse performs well in the presence of J-coupling and tolerates RF miscalibration of up to 4 dB ($\sim$ 45%). Significantly higher bandwidths and/or shorter pulses appear to be attainable. Strategies for obtaining further improvements in pulse performance are considered in the Conclusion.

THEORY

Classical Euler-Lagrange Formalism

Optimal control theory is a generalization (e.g., [20]) of the classical Euler-Lagrange formalism. The goal is to find the curve or trajectory $\boldsymbol{x}(t)$ which optimizes the value of the functional

$$\mathcal{J}[\boldsymbol{x}] = \int_{t_0}^{t_1} \mathcal{L}\,[\,t, \boldsymbol{x}(t), \boldsymbol{u}(t)\,]\,dt \tag{1}$$

over the interval $[\,t_0, t_1]$. In classical mechanics, $\boldsymbol{u} = d\boldsymbol{x}/dt$, $\boldsymbol{x}(t_0)$ and $\boldsymbol{x}(t_1)$ are fixed, and the curves $\boldsymbol{x}(t)$ and $\boldsymbol{u}(t)$ are required to be continuous. The necessary condition that such a curve be an optimizing curve is that the variation $\delta\mathcal{J}$ at all points of the path be equal to zero, which results in the familiar Euler-Lagrange differential equation for the Lagrangian $\mathcal{L}$ [24]. Additional constraints which can be imposed on points of the optimizing curve, of the form $g(\boldsymbol{x}) = c$, are included in the formalism by introducing Lagrange multipliers λ_j for each constraint equation g_j, which transforms the Euler-Lagrange equation for $\mathcal{L}$ to a similar one for the function

$$h = \mathcal{L} - \sum_j \lambda_j g_j. \tag{2}$$

Optimal Control Theory in NMR

For optimal control of a system of noninteracting spins in NMR, the goal is to find the trajectory for the magnetization vector $\boldsymbol{M}(t)$ that optimizes a suitably chosen cost functional $\mathcal{J}$. In units of angular frequency (radians/sec), the effective RF field in the rotating frame is

$$\boldsymbol{\omega}_e = \omega_1(t)\,[\cos\phi(t)\,\hat{\boldsymbol{x}} + \sin\phi(t)\,\hat{\boldsymbol{y}}\,] + \Delta\omega(t)\,\hat{\boldsymbol{z}}, \tag{3}$$

which encompasses any desired modulation of the amplitude ω_1, phase ϕ, and frequency offset $\Delta\omega$ of the pulse. The possible trajectories $\boldsymbol{M}(t)$ are constrained to satisfy the Bloch equation

$$\dot{\boldsymbol{M}} = \boldsymbol{\omega}_e \times \boldsymbol{M}, \tag{4}$$

which therefore introduces three Lagrange multipliers λ_j, as discussed in the previous section. The three constraint functions g_j in Eq. [2] are then simply the components of the vector

$$\boldsymbol{g} = \boldsymbol{\omega}_e \times \boldsymbol{M}. \tag{5}$$

Since $\boldsymbol{\omega}_e(t)$ controls the evolution of $\boldsymbol{M}(t)$, the goal of finding the optimum trajectory is the same as finding the

optimal RF sequence to apply to the sample. Given an initial state $\boldsymbol{M}(t_0)$ and a desired final or target state $\boldsymbol{F}$ at the end of the pulse, we want to optimize

$$\mathcal{J}[\boldsymbol{M}] = \int_{t_0}^{t_p} \mathcal{L}[\,t, \boldsymbol{M}(t), \boldsymbol{\omega}_e(t)\,]\,dt + \Phi[\,\boldsymbol{M}(t_p)\,] \quad (6)$$

over the interval $[t_0, t_p]$. Compared to Eq. [1], we now have $\boldsymbol{u} = \boldsymbol{\omega}_e$. Typically, the "running" cost function $\mathcal{L}$ is chosen with no explicit dependence on $\boldsymbol{M}$ or t. In addition, a final cost term $\Phi(\boldsymbol{M})$ evaluated at the end of the pulse is generally included.

A more significant generalization for the development of optimal control theory is the removal of the restriction that $\boldsymbol{u}$ be continuous. For practical NMR applications, the RF amplitude, phase, and/or frequency must be allowed to make discontinuous jumps. Inclusion of this more general class of piecewise continuous functions merely constrains the proof of the theorem [17] defining the necessary conditions for an optimal solution, as noted in Ref. [20]. The end result is similar to the classical case. Including the Bloch equation constraint on $\boldsymbol{M}$, the requirement $\delta\mathcal{J} = 0$ implies

$$\dot{\boldsymbol{\lambda}} = -\partial h/\partial \boldsymbol{M} \quad (7)$$

with initial condition

$$\boldsymbol{\lambda}(t_p) = \partial\Phi/\partial \boldsymbol{M} \quad (8)$$

for the time evolution of $\boldsymbol{\lambda}$, and

$$\partial h(t)/\partial \boldsymbol{\omega}_e(t) = 0, \quad (9)$$

at all points on the optimal trajectory, which provides a means for adjusting the RF controls. By analogy with the Hamiltonian formalism of classical mechanics, $\boldsymbol{M}$ and $\boldsymbol{\lambda}$ are conjugate variables, since

$$\begin{aligned} \dot{\boldsymbol{M}} &= \boldsymbol{\omega}_e \times \boldsymbol{M} \\ &= \partial h/\partial \boldsymbol{\lambda} \end{aligned} \quad (10)$$

according to Eqs. [2] and [5].

Application to Excitation

For an excitation pulse, the initial state $\boldsymbol{M}(t_0) = \hat{\boldsymbol{z}}$ and the target state $\boldsymbol{F} = \hat{\boldsymbol{x}}$. For the preliminary application of optimal control theory reported here, the running cost, given by the function $\mathcal{L}$ in Eq. [6], was set equal to zero. We then find the optimization of the final cost $\mathcal{J} = \Phi[\,\boldsymbol{M}(t_p)\,]$ has an especially simple geometrical interpretation for the particular choice

$$\Phi = \boldsymbol{M}(t_p) \cdot \boldsymbol{F}, \quad (11)$$

which quantifies the degree to which $\boldsymbol{M}(t_p) = \boldsymbol{F}$. In this case, Eq. [2] becomes

$$h = \boldsymbol{\lambda} \cdot (\boldsymbol{\omega}_e \times \boldsymbol{M}) = \boldsymbol{\omega}_e \cdot (\boldsymbol{M} \times \boldsymbol{\lambda}), \quad (12)$$

Eq. [8] gives

$$\boldsymbol{\lambda}(t_p) = \boldsymbol{F}, \quad (13)$$

and the conditions that must be satisfied at each time for the cost to be maximized are

$$\dot{\boldsymbol{M}} = \boldsymbol{\omega}_e \times \boldsymbol{M}, \qquad \boldsymbol{M}(t_0) = \hat{\boldsymbol{z}} \quad (14)$$

$$\dot{\boldsymbol{\lambda}} = \boldsymbol{\omega}_e \times \boldsymbol{\lambda}, \qquad \boldsymbol{\lambda}(t_p) = \hat{\boldsymbol{x}} \quad (15)$$

$$\frac{\partial h}{\partial \boldsymbol{\omega}_e} = \boldsymbol{M} \times \boldsymbol{\lambda} = 0 \quad (16)$$

As illustrated in Fig. 1, a sequence which transforms $\boldsymbol{M}(t_0)$ forward in time to the desired target state $F = \hat{\boldsymbol{x}}$ therefore transforms $\boldsymbol{\lambda}(t_p) = \boldsymbol{F}$ backwards in time to $\boldsymbol{M}(t_0)$. For the optimal pulse, we then have $\boldsymbol{M}_{\rm opt}(t) = \boldsymbol{\lambda}_{\rm opt}(t)$, which satisfies the stationary condition given by Eq. [16]. For a nonoptimal pulse, $(\boldsymbol{M} \times \boldsymbol{\lambda})$ at each time point of the two trajectories gives the proportional adjustment to make in the control field $\boldsymbol{\omega}_e(t)$.

Herein lies the power and efficiency of optimal control theory. For a m-component control field digitized in n time increments, the final cost Φ to be optimized is a function of $N = mn$ variables. Many methods exist for finding an extremum (minimum or maximum) of an N-dimensional function (see, for example, [25]). Typically, they utilize various strategies for stepping downhill (uphill) until a minimum (maximum) of the function is reached. The extremum found might only be a local rather than global extremum, but this limitation is imposed more by the multidimensional nature of the function than the optimization procedure. A general function, with no closed form analytical expression for calculating the gradient (i.e., the direction of steepest descent), can require on the order of N evaluations to take a single effective step towards the extremum. Each evaluation of the cost function we want to optimize requires, in turn, a time evolution of the initial state over the sequence of control fields. By contrast, optimal control theory requires only the two evolutions shown in Fig. 1 to determine the best direction to step and improve the cost.

Including the Bloch equation as a constraint in the optimization has provided, *for arbitrary RF sequence and cost function*, a quantitative measure of the difference between the evolution of the initial state and $\boldsymbol{\lambda}(t_p)$. As noted in Eq. [8], $\boldsymbol{\lambda}(t_p)$ is directly related to the final cost and equals the target state for the particular choice of Φ in Eq. [11]. One need not make N samples of the parameter space to determine how to drive the initial state to the target state. Depending on the length of the RF sequence, N can easily be on the order of 1000 or more, especially for shaped pulses. Optimal control theory therefore provides an enormous efficiency gain compared to traditional procedures and opens the door to a host of problems that otherwise might be too computationally intensive to be tractable.

Numerical Algorithm

The procedure for optimizing the cost can be incorporated in the following algorithm:

i) Choose an initial RF sequence $\boldsymbol{\omega}_e^{(0)}$.

ii) Evolve $\boldsymbol{M}$ forward in time from the initial state $\hat{\boldsymbol{z}}$.

iii) Evolve $\boldsymbol{\lambda}$ backwards in time from the target state $\hat{\boldsymbol{x}}$.

iv) $\boldsymbol{\omega}_e{}^{(k+1)}(t) \rightarrow \boldsymbol{\omega}_e{}^{(k)}(t) + \epsilon\,[\,\boldsymbol{M}(t) \times \boldsymbol{\lambda}(t)\,]$

v) Repeat steps ii)–iv) until a desired convergence of Φ is reached.

The Bloch equation represents an instantaneous rotation about $\boldsymbol{\omega}_e(t)$. Rotations preserve both the length of vectors and the angles between vectors, so step iii) can be replaced by

iii′) Calculate $\boldsymbol{M}(t_p) \times \boldsymbol{\lambda}(t_p)$ and evolve it backwards in time

which eliminates repeated calculation of $(\boldsymbol{M} \times \boldsymbol{\lambda})$ at each t in step iv).

Broadband Excitation

The ideal cost, $\boldsymbol{M}_x(t_p) = 1$, which is necessary to satisfy Eq. [16] and terminate the algorithm, can not be achieved by an optimal sequence at all resonance offsets simultaneously. For a range of chemical shift offsets, and also a range of nonideal RF fields, the average cost $\langle \boldsymbol{M}_x(t_p) \rangle < 1$. Therefore, the value of $\boldsymbol{M} \times \boldsymbol{\lambda}$ is calculated for each combination of resonance offset and RF field, and the average of all these values, $\langle \boldsymbol{M} \times \boldsymbol{\lambda} \rangle$, is used in step iii′), since it can converge to zero and terminate the algorithm. Effectively, the same result is obtained in Refs. [21, 22], which start with the Bloch equation in matrix form [26] and derive equations equivalent to Eqs. [14–15] using an extended magnetization vector composed of $\boldsymbol{M}$ for each resonance offset. In the present case, the range of RF variation would also be included. The stationary condition in this extended matrix formulation can then be shown to be a sum of Eq. [16] over the offsets. Although the matrix form is entirely equivalent to the vector equations presented here, the straightforward geometric interpretation of Eqs. [14–16] and Fig. 1 is less evident in [21, 22].

There is also no guarantee that the cost is optimized by a sequence satisfying the conditions of Eqs. [14–16]. They are only the necessary conditions. However, since the maximum possible cost for an ideal or perfect broadband excitation pulse is equal to one, the degree to which the cost approaches this value is a practical measure for the utility of its associated RF sequence. We therefore employ the term "optimal" to mean a sequence which satisfies the necessary conditions with a cost that is useful for NMR applications. Proving that it is the best of all possible sequences becomes less important from an applications standpoint as the cost approaches the ideal value.

Since frequency modulation is equivalent to phase modulation, with $\Delta\omega(t) = d\phi(t)/dt$, we considered only amplitude and phase modulation in the current implementation of the algorithm. The value of $\Delta\omega$ in Eq. [3] is then time-independent, and gives the chemical shift of the irradiated spin. A sequence of random (x, y) amplitudes was generated to initiate the algorithm in step i). The two RF control fields $(\boldsymbol{\omega}_1)_x$ and $(\boldsymbol{\omega}_1)_y$ were digitized in 0.5 μs steps over the 2 ms pulse length. RF inhomogeneity in the amplitude $\omega_1(t)$ was incorporated by scaling the ideal RF amplitude $\omega_1^0(t)$ according to $\omega_1(t) = \alpha\,\omega_1^0(t)$ for constant factors α.

Using steps ii) and iii′), the average $\langle \boldsymbol{M} \times \boldsymbol{\lambda} \rangle$ was calculated over a combination of 81 resonance offsets in the range ± 20 kHz, incremented by 500 Hz, and 5 RF scalings given by $\alpha = (0.95, 0.975, 1.0, 1.025, 1.05)$. The RF values were weighted according to a Gaussian distribution $\exp[-(1-\alpha)^2/(2\sigma^2)]$, with $\sigma = 0.042$ giving a full width at half-maximum (FWHM) of 0.1, or 10% of the nominal RF value. The resonance offsets were weighted equally.

As noted, only the transverse or (x, y) components of $\boldsymbol{\omega}_e$ were modified in step iv). This effectively ignores the information contained in the z component of $\boldsymbol{M} \times \boldsymbol{\lambda}$ for optimizing the cost. The stepsize, ϵ, can be chosen sufficiently small to ensure the solution always tends steadily towards the optimum, but this can be overly time-consuming, involving many unnecessarily small steps during some iterations. Instead, the largest step providing improvement in the cost was determined at each iteration by bracketing the optimal step size among three values and using a simple 1D line minimization routine [25]. The efficiency of the optimization was further enhanced using a conjugate gradient method to determine the step direction. The maximum amplitude of the RF controls was constrained indirectly by the fixed pulse length, with $t_p = 2$ ms resulting in an optimized pulse amplitude $B_1(t) = \omega_1(t)/(2\pi)$ less than 20 kHz. Our cost function, with a total of 8000 independent control parameters to be optimized over 405 possible combinations of RF scale factor and resonance offset, would present a formidable challenge for the traditional optimization methods mentioned earlier.

RESULTS AND DISCUSSION

The optimal control algorithm, implemented according to the design criteria of the previous section, converged to the excitation pulse displayed in Fig. 2. The algorithm requires less than 30 minutes of CPU time to generate the pulse on a 1.5 GHz Pentium IV processor. The seemingly random appearance of the pulse belies its function: each increment of the pulse delivers the precise RF amplitude and phase required to maximize the final x magnetization over the target ranges in RF inhomogeneity and resonance offset for the given (random) initial RF waveform. The inverse transformation $I_x \rightarrow I_z$ can be obtained by applying the time-reversed pulse, with each phase incremented by 180°.

The theoretical performance of the pulse, assuming simple Bloch equation evolution of the irradiated spins (as in

the optimization procedure), is illustrated in Fig. 3. Contours of x magnetization, M_x, are plotted in the upper panel as functions of resonance offset and RF inhomogeneity. The phase of the excited magnetization is shown similarly in the lower panel. Over a $\pm 5\%$ variation in the nominal RF delivered by the coil and resonance offsets of ± 20 kHz, the excited magnetization M_x is at least 99.5% of the initial z magnetization, M_0. Although the optimization was not performed outside these stated ranges, nonetheless $M_x/M_0 >\sim 99\%$ over a $\pm 10\%$ variation in RF, and the phase of the final magnetization is less than $\sim 8^\circ$ over this larger RF range, operating over the same 40 kHz bandwidth.

The FOM of 2.3 for this pulse is comparable to the best values of the previous broadband excitation pulses, with the exception of the 12 ms ABSTRUSE pulse, which gives a much higher FOM at the price of increased vulnerability to J-coupling and relaxation effects. The FOM, however, provides no measure for the uniformity of the performance as a function of changing RF calibration or homogeneity. The optimal control algorithm has produced exceptional results over the targeted parameter range (± 20 kHz resonance offset, $\pm 5\%$ RF inhomogeneity). Since the other pulses were designed with only resonance offset performance as a consideration, a more illuminating comparison might be obtained by applying optimal control theory to the design of broadband excitation with only ideal RF values used in the algorithm. In such a case, simulations (not shown) of the resulting pulse performance show nearly perfect excitation, $I_z \rightarrow 0.999\, I_x$, over a bandwidth of 100 kHz with FOM = 5.2. This is more than double the value for Fig. 3, and requires only a modest $\sim 10\%$ increase in peak RF amplitude. As expected, however, the tolerance to RF variability is poorer, with M_x dropping to 90% of M_0 at a $\pm 5\%$ change in the nominal RF delivered by the coil over resonance offsets of ± 50 kHz. Nonetheless, this example illustrates there is considerable scope for improving pulse performance without increasing peak power and also emphasizes the FOM as defined is a relatively limited measure of performance.

The longer an excitation pulse is, the more important the potential effects of J-coupling during the pulse, and 2 ms is sufficiently long that this could be a significant concern. Separate simulations of a heteronuclear 2-spin system (J = 150 Hz) and a homonuclear system (J = 55 Hz) produced results equivalent to those shown in Fig.3 for an uncoupled system. All systems were simulated starting with initial z magnetization (the total magnetization of both spins in the homonuclear case). Experimental confirmation of the utility of the pulse for realistic applications involving excitation of coupled spin systems is provided in Fig. 4. The ^{13}C spectrum of $\sim$ 20 mM 100% ^{13}C-labeled lysine exhibits only minimal phase distortions, either from resonance offset effects, C-C couplings, or H-C couplings. On the 800 MHz spectrometer employed, the 40 kHz bandwidth of the pulse is sufficient to excite the full 200 ppm (40.24 kHz) ^{13}C chemical shift range. In general, the broadband capabilities of relatively long excitation pulses have to be examined carefully to determine whether they are applicable to both coupled and uncoupled systems.

To verify the stability of the pulse with respect to RF-miscalibration, as well as its scalability, a series of excitation offset profiles were acquired with power levels (dB) set to -2, -1, 0, 1 and 2 dB relative to the calibrated excitation pulse. The pulse was scaled by a factor of 2, doubling the pulse length and halving the RF amplitude. Offset profiles were thus recorded using a 4 ms version of the excitation pulse with a maximum RF amplitude of 8774 Hz, giving a bandwidth of ± 10 kHz. In Fig. 5, the optimized excitation bandwidth is achieved for the whole 4 dB range ($\sim 45\%$), with an excitation amplitude for all offsets and power levels $> 83\%$ of the maximum value within the range and a maximum phase distortion of less than 17°.

The broadband excitation pulse was implemented on a Bruker DMX 800 spectrometer equipped with modern SGU units for RF-control and linearized amplifiers. Initial trials were performed on a DMX 500 spectrometer with non-linearized amplifiers which resulted in resonable excitation profiles but a significant improvement was evident on the DMX 800 spectrometer with a more modern console and linearized amplifiers. We therefore highly recommend the use of amplitude- and phase-linearized amplifiers in order to achieve best results.

Finally, scaling the RF power to the maximum allowed by the system hardware produced the result shown in Fig. 6. The pulse length is 1.25 ms and the maximum RF amplitude is 28.1 kHz, giving a bandwidth of 64 kHz. Values for the amplitude and phase of the excited magnetization over the bandwidth of the pulse are consistent with the simulations of Fig. 3. In this case the pulse was digitized in very short steps of 0.3125 μs, but the handling of the waveform generator on the DMX 800 spectrometer still gives excellent results with the excitation amplitude generally higher than 93% and phase distortions less than 8°.

CONCLUSION

Optimal control theory provides a systematic and flexible formalism that can be readily applied to pulse sequence design. To illustrate the utility of the procedure, we have presented a 2 ms implementation of *B*roadband *E*xcitation *B*y *O*ptimized *P*ulses (BEBOP), that performs well in the presence of J-coupling and is tolerant to the range of RF miscalibration typical in high resolution NMR. For a peak RF amplitude of 17.5 kHz, it produces final magnetization of approximately uniform phase over a resonance offset range of 40 kHz with a tolerance of $\sim 45\%$ to RF miscalibration. Over the targeted range of RF variability, the phase is $< 4^\circ$. Pulse performance at both lower and higher power has also been demonstrated, giving excita-

tion bandwidths of 20 kHz and 64 kHz, respectively. We also mentioned in passing a 2 ms pulse designed without consideration for RF tolerance that achieves an excitation bandwidth of 100 kHz for the ideal RF values used in its design (peak RF = 19.4 kHz).

BEBOP was obtained using a particularly straightforward implementation of optimal control theory, and as such, merely scratches the surface of what is possible. The optimization produces pulses of exceptional quality for the targeted ranges of resonance offset and RF variability. Testing the limits of pulse performance is the next order of business. It would be useful, for example, to obtain shorter pulses in order to minimize relaxation effects. Maximizing excitation bandwidth as a function of peak RF amplitude is important, and the limits of tolerance to RF inhomogeneity need to be explored. Design of plane rotation pulses (universal rotors) is also a logical next step. All these goals should be pursued without increasing RF amplitudes above the limits available for ^{13}C spectroscopy. One possibility is to assign a running cost $\mathcal{L} = \beta\omega_e{}^2(t)$ in Eq. [6], with the weight β determining the penalty for larger RF values. Other expressions for the final cost Φ are also possible. Another strategy would be to clip the RF amplitude at a desired maximum value and force the optimal control algorithm to search for another solution whenever the amplitude exceeds this limit. While these possibilities are being investigated, the 2 ms BEBOP can be downloaded in the interim from http://www.org.chemie.tu-muenchen.de/people/bulu/.

ACKNOWLEDGMENTS

T.E.S. was supported by The Wright State University while on sabbatical leave (2001–2002 academic year) at Technische Universität München. B.L. thanks the Fonds der Chemischen Industrie and the Deutsche Forschungsgemeinschaft (Emmy Noether fellowship LU 835/1-1) for support. S.J.G. acknowledges support from the Deutsche Forschungsgemeinschaft for Grants Gl 203/3-1 and Gl 203/4-1 and the Fonds der Chemischen Industrie. N.K. would like to acknowledge Darpa Grant F49620-0101-00556.

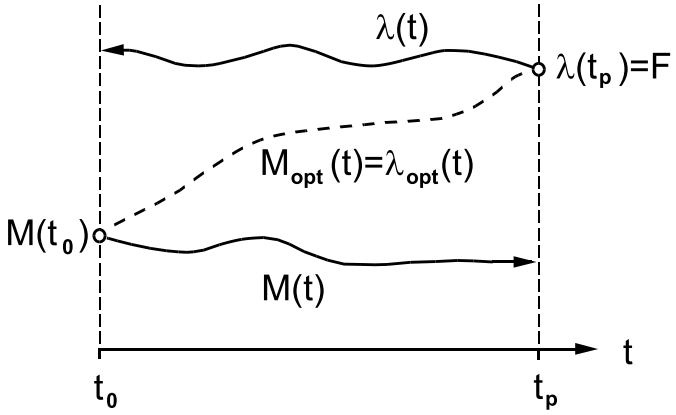

FIG. 1. Optimization scheme. For a given RF sequence $\boldsymbol{\omega}_e(t)$, the initial state $\boldsymbol{M}(t_0)$ evolves to some final state $\boldsymbol{M}(t_p)$ through a sequence of intermediate states, shown schematically as the solid line connecting $\boldsymbol{M}(t_0)$ and $\boldsymbol{M}(t_p)$. Similarly, the desired final target state $\boldsymbol{F}$, which is equal to the Lagrange multiplier term $\boldsymbol{\lambda}(t_p)$ according to Eqs. [8] and [11], evolves backwards in time to some initial state $\boldsymbol{\lambda}(t_0)$. The separate paths for $\boldsymbol{M}(t)$ and $\boldsymbol{\lambda}(t)$ become equal for the optimized RF sequence $\boldsymbol{\omega}_{\rm opt}(t)$ that drives $\boldsymbol{M}(t_0)$ to $\boldsymbol{\lambda}(t_p) = \boldsymbol{F}$. At each time, a comparison of the two paths via $\boldsymbol{M}(t)\times\boldsymbol{\lambda}(t)$ gives the proportional adjustment to make in each component of the control field $\boldsymbol{\omega}_e(t)$ to bring the two paths closer together.

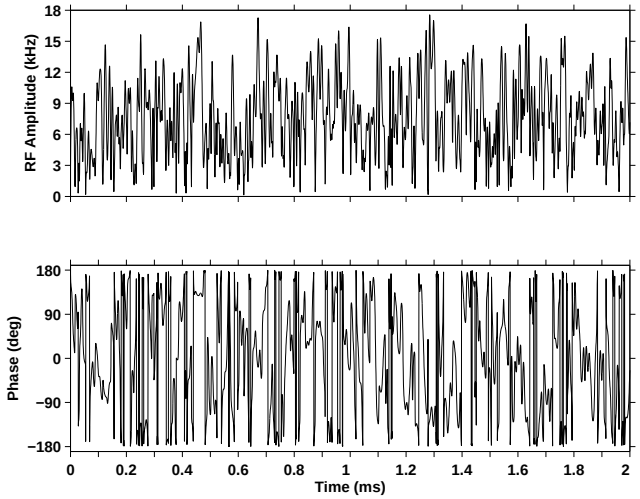

FIG. 2. Broadband excitation pulse. The deceptively "random" appearance in pulse amplitude (upper panel) and phase (lower panel) as a function of time efficiently choreographs the transformation $I_z \rightarrow I_x$ over a 40 kHz range of resonance offsets with moderate tolerance to RF miscalibration (see Fig. 3). The pulse length was fixed at 2 ms, resulting in a maximum RF amplitude for the pulse of 17.5 kHz. A 2 ms pulse of constant 8.5 kHz RF amplitude would have the same power requirements as the pulse shown.

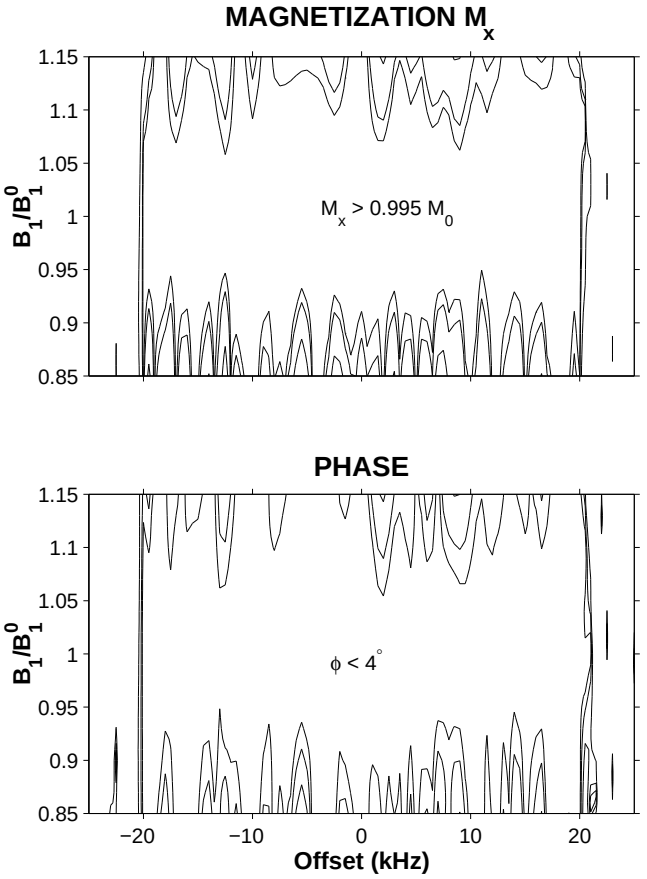

FIG. 3. Simulated performance of the optimized pulse of Fig. 2. Starting with initial z magnetization M_0, the magnitude M_x (upper panel) and phase ϕ (lower panel) of the excited magnetization is plotted as a function of resonance offset and RF field B_1, represented as a fraction of the nominal field B_1^0. Contour lines displayed for M_x are [0.995, 0.99, 0.96], and those for the phase of the excited magnetiztion are [4°, 8°, 16°]. Contours similar to those shown above are obtained for homonuclear and heteronuclear scalar-coupled systems, as discussed in the text. In comparison, a hard 90° pulse ("peak" RF amplitude equal to 17.5 kHz, as above), after linear phase correction of the spectrum, gives $M_x > 0.995\, M_0$ over offsets of only ± 6 kHz for $0.95 \leq B_1/B_1^0 \leq 1.05$ and ± 12 kHz for $B_1/B_1^0 = 1$.

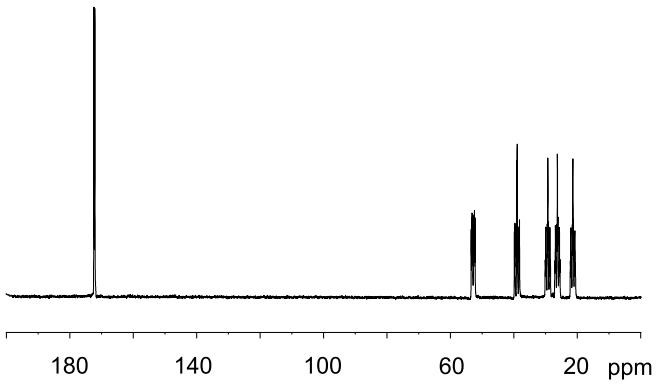

FIG. 4. 800 MHz ^{13}C spectrum of 100% ^{13}C-labeled lysine. The spectrum was acquired after irradiation of the sample with the pulse shown in Fig. 2. The delay between the 90° pulse and the first data point of the FID was set to the dwell time in order to obtain the pure phase behavior of the excitation pulse. The acquired spectrum is an average of 64 scans, exponentially apodized and 0th order phase corrected. No 1st order phase correction was applied. The phase of the spectrum is uniform over the full ^{13}C chemical shift range, and effects due to C-C or H-C couplings during the 2 ms application of the pulse are minimal.

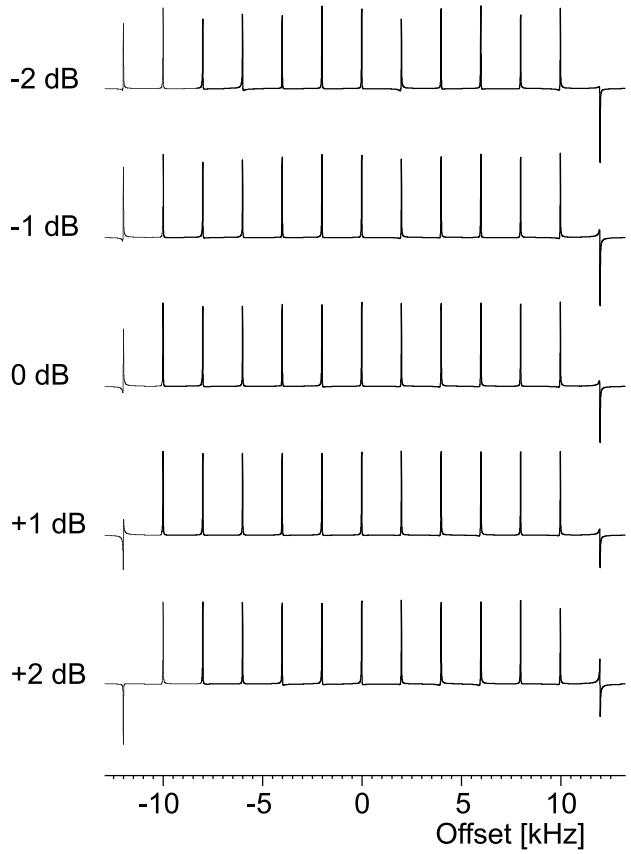

FIG. 5. Excitation profiles for the residual HDO signal in a sample of 99.9% D_2O are displayed as a function of resonance offset and RF power levels applied to the sample for a 4 ms pulse obtained by scaling all RF values in the optimized pulse of Fig. 2 by 1/2. The pulse has a maximum RF amplitude of 8774 Hz in the calibrated case (0 dB), with RF power levels set to ± 1 and ± 2 dB relative to the calibrated pulse. The broadband excitation pulse is relatively insensitive to pulse miscalibration over the 4 dB range, corresponding to a $\sim 45\%$ variability in the RF calibration.

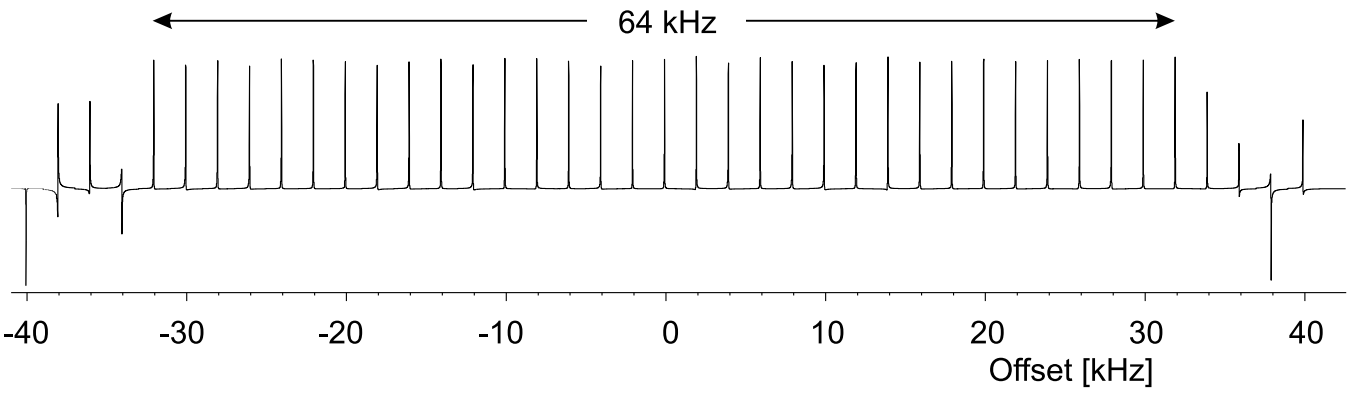

FIG. 6. Excitation offset profile of a 1.25 ms broadband excitation pulse, obtained by scaling the pulse of Fig. 2 to the maximum RF of 28.1 kHz available on the system hardware. The amplitude of the excited magnetization is $> 93\%$ over the complete bandwidth of 64 kHz and phase distortions are generally less than $8°$.

REFERENCES

1. R. Freeman, S. P. Kempsell, and M. H. Levitt, Radiofrequency pulse sequences which compensate their own imperfections, *J. Magn. Reson.* **38**, 453–479 (1980).
2. M. H. Levitt, Symmetrical composite pulse sequences for NMR population inversion. I. Compensation of radiofrequency field inhomogeneity, *J. Magn. Reson.* **48**, 234–264 (1982).
3. M. H. Levitt and R. R. Ernst, Composite pulses constructed by a recursive expantion procedure, *J. Magn. Reson.* **55**, 247–254 (1983).
4. R. Tycko, H. M. Cho, E. Schneider, and A. Pines, Composite pulses without phase distortion, *J. Magn. Reson.* **61**, 90–101 (1985).
5. M. H. Levitt, Composite pulses, *Prog. Nuc. Magn. Reson. Spectrosc.* **18**, 61–122 (1986).
6. A. J. Shaka and A. J. Pines, Symmetric phase-alternating composite pulses, *J. Magn. Reson.* **71**, 495-503 (1987).
7. J.-M. Böhlen, M. Rey, and G. Bodenhausen, Refocusing with chirped pulses for broadband excitation without phase dispersion, *J. Magn. Reson.* **84**, 191–197 (1989).
8. J.-M. Böhlen and G. Bodenhausen, Experimental aspects of chirp NMR spectroscopy, *J. Magn. Reson. Series A* **102**, 293–301 (1993).
9. D. Abramovich and S. Vega, Derivation of broadband and narrowband excitation pulses using the Floquet Formalism, *J. Magn. Reson. Series A* **105**, 30–48 (1993).
10. Ē. Kupče and R. Freeman, Wideband excitation with polychromatic pulses, *J. Magn. Reson. Series A* **108**, 268–273 (1994).
11. K. Hallenga and G. M. Lippens, A constant-time ^{13}C–^{1}H HSQC with uniform excitation over the complete ^{13}C chemical shift range, *J. Biomol. NMR* **5**, 59-66 (1995).
12. T.-L. Hwang, P. C. M. van Zijl, and M. Garwood, Broadband adiabatic refocusing without phase distortion, *J. Magn. Reson.* **124** 250–254 (1997).
13. K. E. Cano, M. A. Smith, and A. J. Shaka, Adjustable, broadband, selective excitation with uniform phase, *J. Magn. Reson.* **155**, 131-139 (2002).
14. L. Allen and J. H. Eberly, "Optical Resonance and Two-Level Atoms," Wiley, New York (1975).
15. J. Baum, R. Tycko, and A. Pines, Broadband and adiabatic inversion of a two-level system by phase-modulated pulses, *Phys. Rev. A* **32**, 3435–3447 (1985).
16. J. S. Silver, R. I. Joseph, and D. I. Hoult, Selective spin inversion in nuclear magnetic resonance and coherent optics through an exact solution of the Bloch-Ricatti equation, *Phys. Rev. A* **31**, 2753-2755 (1985).
17. L. Pontryagin, B Boltyanskii, R. Gamkrelidze, and E. Mishchenko, "The Mathematical Theory of Optimal Processes," Wiley-Interscience, New York (1962).
18. A. P. Sage, "Optimum Systems Control," Prentice-Hall, Inc., Englewood Cliffs, N.J. (1968).
19. A. Bryson, Jr. and Y.-C. Ho, "Applied Optimal Control," Hemisphere, Washington, D.C. (1975).
20. E. Pinch, "Optimal Control and the Calculus of Variations," Oxford University Press, Oxford (1993).
21. S. Conolly, D. Nishimura, and A. Macovski, Optimal control solutions to the magnetic resonance selective excitation problem, *IEEE Trans. Med. Imag.* **MI-5**, 106–115 (1986).
22. D. Rosenfeld and Y. Zur, Design of adiabatic selective pulses using optimal control theory, *Magn. Reson. Med.* **36**, 401–409 (1996).
23. J. T. Ngo and P. G. Morris, General solution to the NMR excitation problem for noninteracting spins, *Magn. Reson. Med.* **5**, 217–237 (1987).
24. H. Goldstein, "Classical Mechanics," Addison-Wesley, Reading, MA (1980).
25. W. H. Press, S. A. Teukolsky, W. T. Vetterling, and B. P. Flannery, "Numerical Recipes in C," Cambridge University Press, New York, NY (1988).
26. E. T. Jaynes, Matrix treatment of nuclear induction, *Phys. Rev.* **98**, 1099–1105 (1955).